`Supplementary Material

Z-scheme heterojunction g-C$_3$N$_4$/CQDs/CdZnS with high redox capability for enhancing visible light-driven photocatalytic depolymerization of lignin into aromatic monomers

Xutang Liu[1, a], Zhijie Jiang[1, a], Xiru Cao[a], Zhen Shen[b, *], Wei Zhao[a, *], Fei Wang[a], Mingyu Cui[c], Chong Liang[a]

[a] School of Chemical Engineering and Technology, China University of Mining & Technology, Xuzhou, 221116, Jiangsu, China

[b] School of Chemistry and Chemical Engineering, Nanjing University, Nanjing 210023, Jiangsu, China

[c] State Key Laboratory of Materials Processing and Die & Mould Technology, School of Materials Science and Engineering, Huazhong University of Science and Technology, Wuhan, 430074, China

*Corresponding authors: shenzhen18305@163.com (Z. Shen), zhaow1965@163.com (W. Zhao).

[1] These authors contributed equally to this work.

SI-1. Catalyst characterization

X-ray diffractometer (XRD, Bruker D8 ADVANCE, Germany) was employed to analyze the crystal phase with Cu-Kα radiation (λ = 1.5406 Å). The molecular weight of extracted lignin was characterized by gel permeation chromatography (Shimadzu, Japan). The surface morphology of catalysts was observed by field-emission scanning electron microscopy (FESEM, TESCAN MAIA3 LMH, Czech Republic) and the element composition was determined by energy dispersive spectroscopy (EDS, IXRF Systems Model 550i, USA). Microstructure and lattice spacing was observed by field emission transmission electron microscope (TEM, FEI Tecnai G2 F20, USA), and high-resolution transmission electron microscope (HETEM) was detected on the same instrument. Fourier transform infrared spectrometer (FT-IR, Thermo NICOLET is5, USA). The functional groups were characterized by Fourier transform infrared spectra (FT-IR, Thermo NICOLET is5, USA) using a KBr pellet method. Chemical composition and states were measured by an X-ray photoelectron spectroscopy (XPS, Thermo ESCALAB 250Xi, USA) with a monochromatic Al-Kα source and spot size of 900 μm. The optical property and bandgap were analyzed by UV-Vis diffuse reflectance spectroscopy (UV-Vis DRS, Persee TU1901, China). Photoluminescence spectrum was recorded on a fluorescence spectrophotometer (PL, Hitachi F-4600, Japan) with an excitation wavelength of 280 nm (λ_{ex} = 280 nm), which can evaluate the recombination efficiency of electrons and holes. The radical intermediates (h^+, ·OH and ·CH_2) were used to detect by Electron spin resonance (ESR, JEOL Bruker EMXPlus-10/12).

The photoelectrochemical tests were measured by an electrochemical workstation (Chenhua CHI 660E, China) equipped with a standard three-electrode cell and 300 W Xe lamp. The details of the tests are as follows: the working electrodes prepared by depositing the photocatalysts on the pre-cleaned indium-tin oxide (ITO) glasses (1 cm × 4 cm), Pt sheet were used as counter electrode and Ag/AgCl electrode was used as reference electrode, and electrolyte was 0.2 M Na_2SO_4 solution. The photocurrent tests were carried out at an initial potential of 0.5 V with the dark/light conditions at 20s intervals. Electrochemical impedance spectroscopy (EIS) curves were obtained through setting the frequency of 0.01-10^5 Hz with the open circuit potential of 0.5 V. The Mott-Schottky curves were recorded at a frequency of 1KHz and scanning the potential of -1.4 ~ -0.2 V.

SI-2. DFT functional theory (DFT) calculations

Periodic spin−polarized density functional theory DFT calculations were performed using the Vienna Ab−initio Simulation Package (VASP version 5.4.4) [1] with the Perdew-Burke-Ernzerhof (PBE) exchange correlation functional [2], a plane-wave basis set with a cutoff kinetic energy of 450 eV and the projector-augmented wave (PAW) method [3]. PAW pseudo-potentials were selected according to the Materials Project (MP) database [4]. The Brillouin zone was sampled with a Γ−centered (5×5×1) Monkhorst-Pack grid [5]. The energy and force convergence criteria were set as 1.0×10^{-5} eV and 0.01 eV Å^{-1}, respectively, with a vacuum space of 20 Å.

The work function of the surface is a crucial parameter in investigating the charge transfer of the interface and semiconductor band alignment. Herein, we calculated the work functions of CZS (111) and monolayer CN (002) surfaces according to the following equation:

$$\Phi = E_{Vac} - E_F$$

where E_{Vac} is the electrostatic potential of the vacuum level and E_F is the Fermi level energy.

SI-3. Extraction of lignin

Birch lignin was extracted according to previous reported [6]. 10 g of pre-ground birch wood and 100 mL methanol containing 3 mL hydrochloric acid (37%) were added to a 100 mL flask. The mixture was refluxed for 12 h under stirring, and cooled to room temperature. Residue was removed by filtration and washed with adding small portions of methanol. The filtrate was concentrated to <10 mL by rotary evaporation and then poured into 200 mL of ice-cold water with vigorous stirring, obtaining a dark brown solid to precipitate. This lignin was collected by filtration, washed with water and dried overnight under vacuum at 60 ℃. Pine lignin was extracted in the same way. Wheat stalk lignin was extracted according to our previous study [7]. 6 g wheat stalk power, 3 mmol of 1-(3-sulfobutyl) triethylammonium hydrogen sulfate and 100 mL solvent of the ethanol/water (v/v = 4/1) were added to a 250 mL stainless-steel autoclave (YZPR-250 (M), Yanzheng instrument Co., Ltd., China) equipped with mechanical agitation (300 rpm). After purging air with nitrogen three times and pressurizing to 1.0 MPa, the reactor was heated to 200 ℃ for 30 min. After that, the mixture was cooled to ambient temperature. Residue was removed by filtration and washed with water. Then 300 mL of water was added to the filtrate for precipitating lignin, which was eventually isolated and dried at 60 ℃.

SI-4. Preparation of lignin model compounds

Preparation of 2-phenoxy-1-phenylethanone (PP-one)
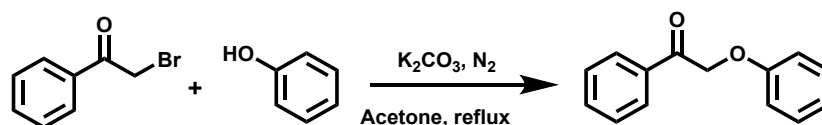
PP-one was prepared by our previous study. A mixture of phenol (25 mmol, 4.98 g) and K_2CO_3 (37.5 mmol, 5.183 g) was dissolved in acetone (60 mL) under stirring at room temperature for 30 min. Then 2-bromoacetophenone (30 mmol, 2.82 g) was added to the mixture solution with N_2 atmosphere and stirred at reflux temperature for 6 h, and then cooled to room temperature. The suspension was collected by filtration and washed with acetone and concentrated under reduced pressure. The crude residue was purified by recrystallization with ethanol to give a white solid **2-phenoxy-1-phenylethanone** (82%).
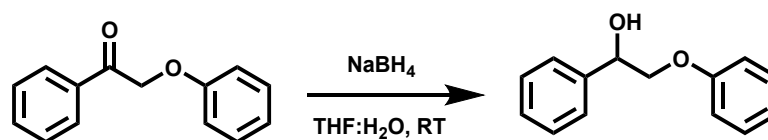
NaBH$_4$ (1.42 g, 37.32 mmol) was slowly added to the solution of 2-phenoxy-1-phenylethanone (4 g, 18.66 mmol) in THF: H_2O (4:1, 50 mL) and stirred at room temperature for 6 h. The reaction was quenched by excess of diluted HCl solution. The coarse product was separated and the aqueous layer was extracted with ethyl acetate. The organic phase was thoroughly washed with NaCl aqueous solution, dried with MgSO$_4$, the residue solid was purified by column chromatography to give product **2-phenoxy-1-phenylethanol** as a white powder (97%). 2-(2-methoxyphenoxy)-1-phenylethanol (PP-ol-MeO) was preparation by the same method. The detailed data were recorded in our previously reported [8].

SI-5. The conversion of lignin model compounds and yield of products
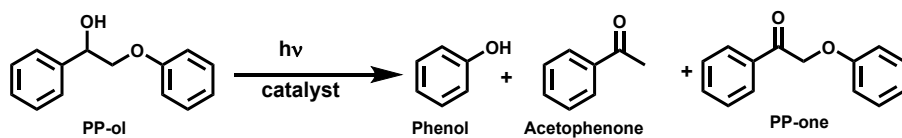
$$\text{Conversion } (\%) = \frac{\text{Moles of reacted substrate}}{\text{Moles of initial substrate}} \times 100$$

$$\text{Yield of phenol } (\%) = \frac{\text{Moles of formed phenol}}{\text{Moles of initial substrate}} \times 100$$

$$\text{Yield of acetophenone } (\%) = \frac{\text{Moles of formed acetophenone}}{\text{Moles of initial substrate}} \times 100$$

$$\text{Yield of PP-one } (\%) = \frac{\text{Moles of formed PP-one}}{\text{Moles of initial substrate}} \times 100$$

Table S1. The fitting results of standard curves of samples by HPLC.

Sample	Regression equation	R^2
Vanillin	$y = 15032.80645x - 7.5625$	0.99999
Vanillic acid	$y = 12656.4086x - 5.59167$	0.99991
PP-ol	$y = 1587.28035x + 11.65194$	0.99956
PP-one	$y = 2404.85978x + 7.46237$	0.99995
Phenol	$y = 5570.46284x + 58.26427$	0.99997
Acetophenone	$y = 4121.36901x + 5.81082$	0.99999

Table S2. Proximate and ultimate analysis of lignin [9].

Sample	Proximate analysis (wt%)[a]				Ultimate analysis (wt%, *daf*)				
	M_d	A_d	V_{daf}	FC_d	C	H	N	S	O[b]
Lignin	5.1	14.3	46.5	37.1	49.0	4.7	0.2	4.1	42

[a] By difference: *daf*, dry and ash-free base; M_d, moisture; A_d, ash; d, dry base; V_{daf}, volatile matter; FC_d, fixed carbon.

[b] The oxygen content was estimated by the conservation of mass according to the assumption that raw lignin contains C, H, N, S and O only.
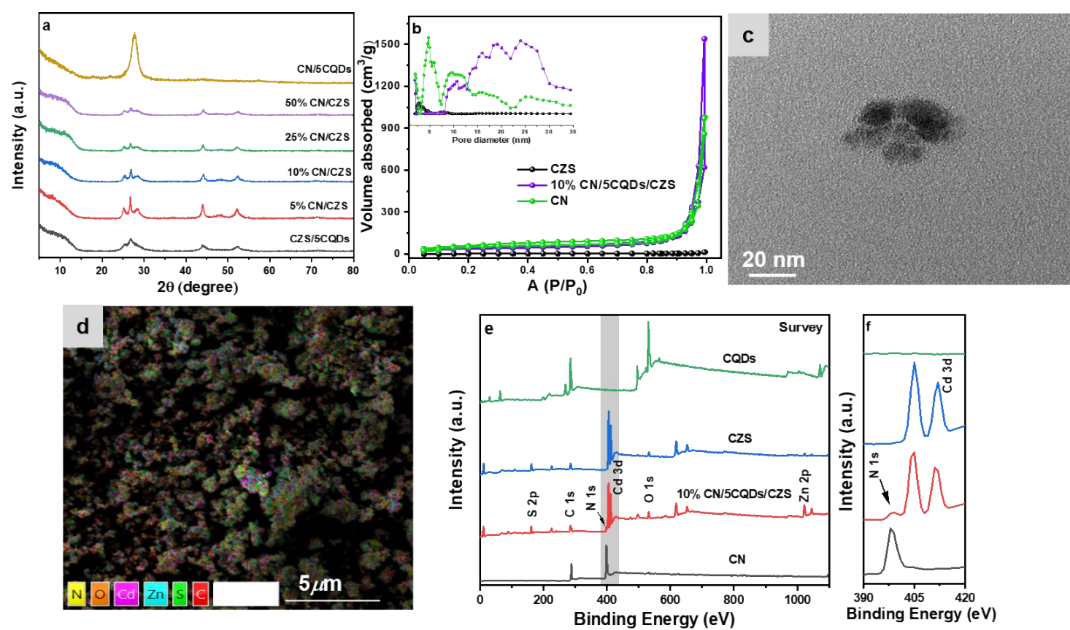
Figure S1. (a) XRD patterns of CN/5CQDs, CZS/5CQDs and CN/CZS composites, (b) N₂ absorption-desorption isotherms and pore size distribution, (c) TEM image of CQDs, (d) EDS image of 10% CN/5CQDs/CZS, (e) XPS survey spectra of CN, CZS and 10% CN/5CQDS/CZS, and (f) is enlarged gray area in (e).
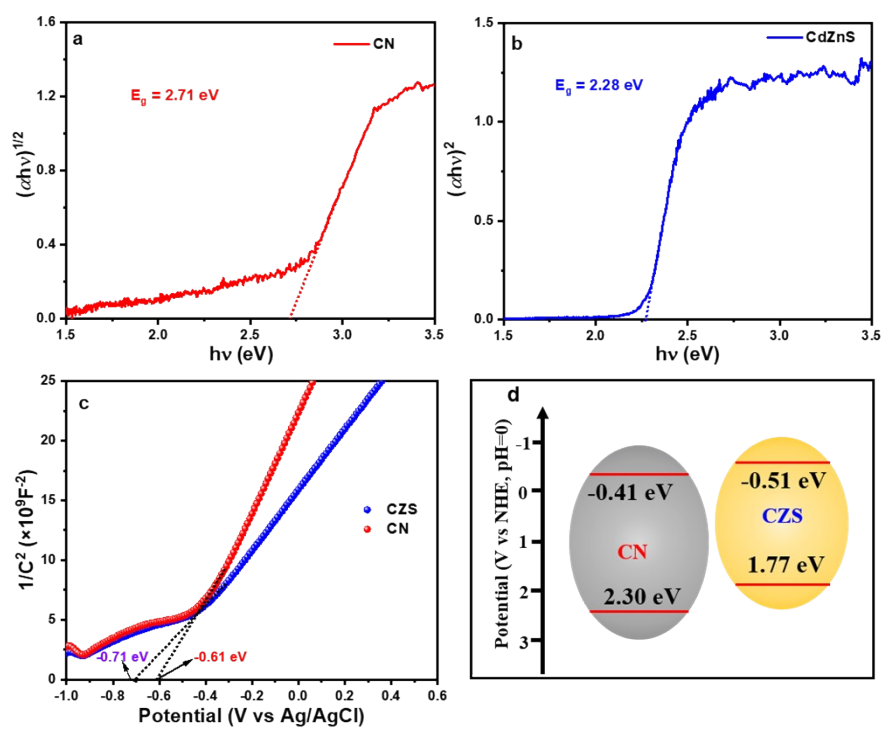
Figure S2. The Kubelka-Munk function plots of CN (a) and CdZnS (b), the Mott-Schottky plots (c) and the energy band structure (d) for CN and CZS.
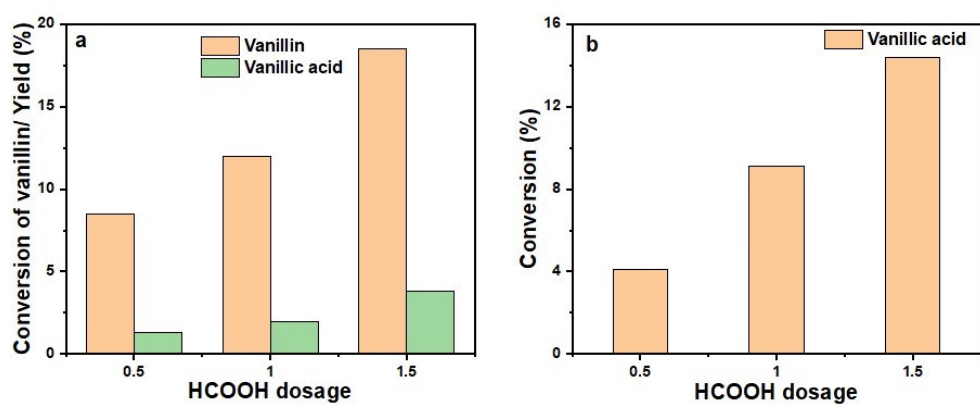
Figure S3. Control experiments with different substrates (a) vanillin and (b) vanillic acid over 10% CN/5CQDs/CZS under visible-light illumination.
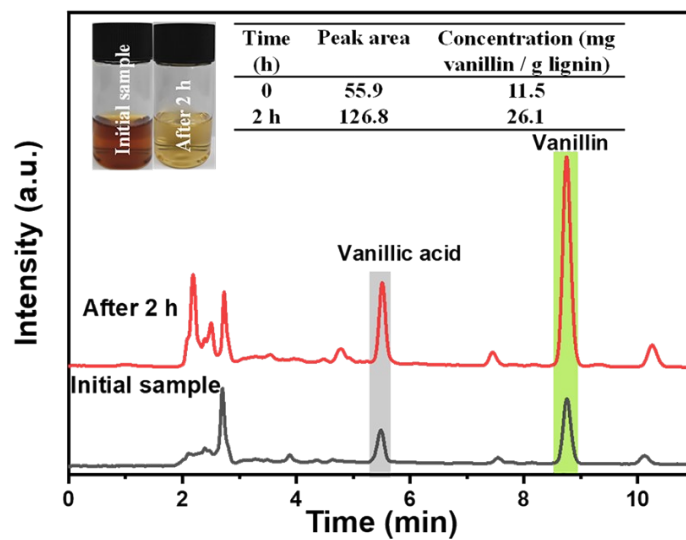
Figure S4. HPLC chromatograms of products from lignin depolymerization.
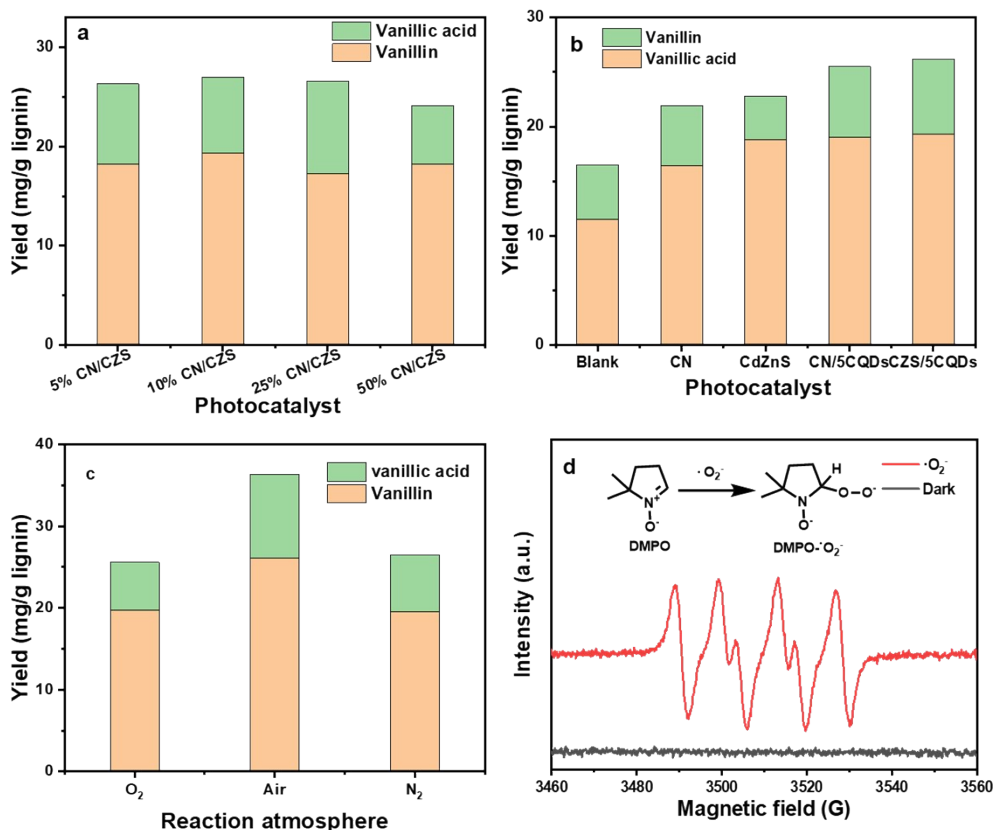
Figure S5. The effect of (a) binary composite photocatalysts, (b) blank experiment without the photocatalysts control experiments of single photocatalysts, (c) reaction atmosphere, (d) DMPO-•O_2^- tests under visible light illumination (10 mg 10%CN/5CQDs/CZS, 1 mL H_2O and 40.0 μL DMPO).
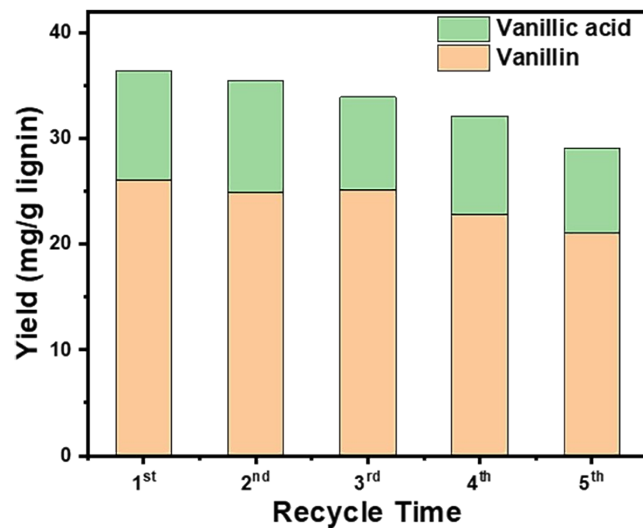
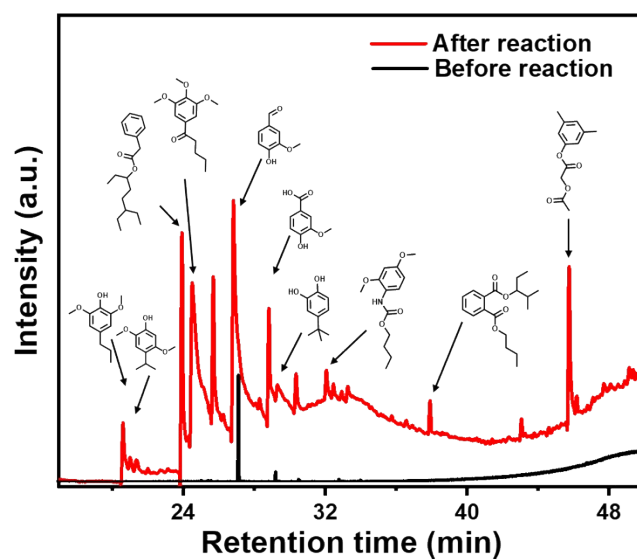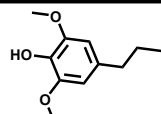**Figure S6.** (a) Recyclability of 10% CN/5CQDS/CZS for photocatalytic lignin depolymerization.
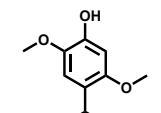
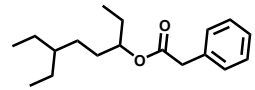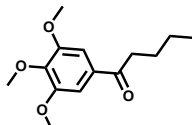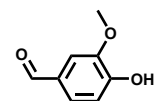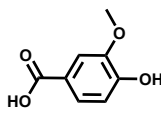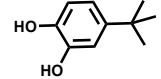**Figure S7.** GC-MS analysis for photocatalytic conversion of dealkaline lignin. Reaction conditions: 50 mg lignin, 50 mg of 10% CN/5CQDS/CZS, 50 mL SDS-8/HCOOH (v/v, 4/1), air atmosphere, 300 W Xe-lamp, 2 h.

Table S3. The products from lignin depolymerization (Identified by GC-MS).

Entry	Compounds	Retention time (min)	Relative content (%)
1		20.59	3.94
2		21.01	1.17
3		23.92	9.65
4		24.51	17.57
5		26.81	42.56
6		28.82	8.64
7		29.35	1.61

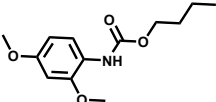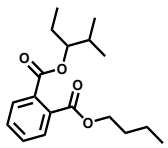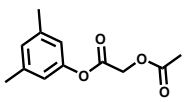|			
8		32.05	2.75
9		37.90	1.51
10		45.739	10.60

Table S4. The average molecular weight of lignin products before and after photocatalytic reaction.

Entry	Types of lignin	M_w (Da)	M_n (Da)	PDI (M_w/M_n)
1	Birch lignin	1934	1487	1.30
2	Pine lignin	2658	1735	1.53
3	Wheat straw lignin	1295	667	1.94
4	Birch lignin after photocatalytic reaction	876	761	1.15
5	Pine lignin after photocatalytic reaction	720	602	1.19
6	Wheat straw lignin after photocatalytic reaction	648	614	1.06

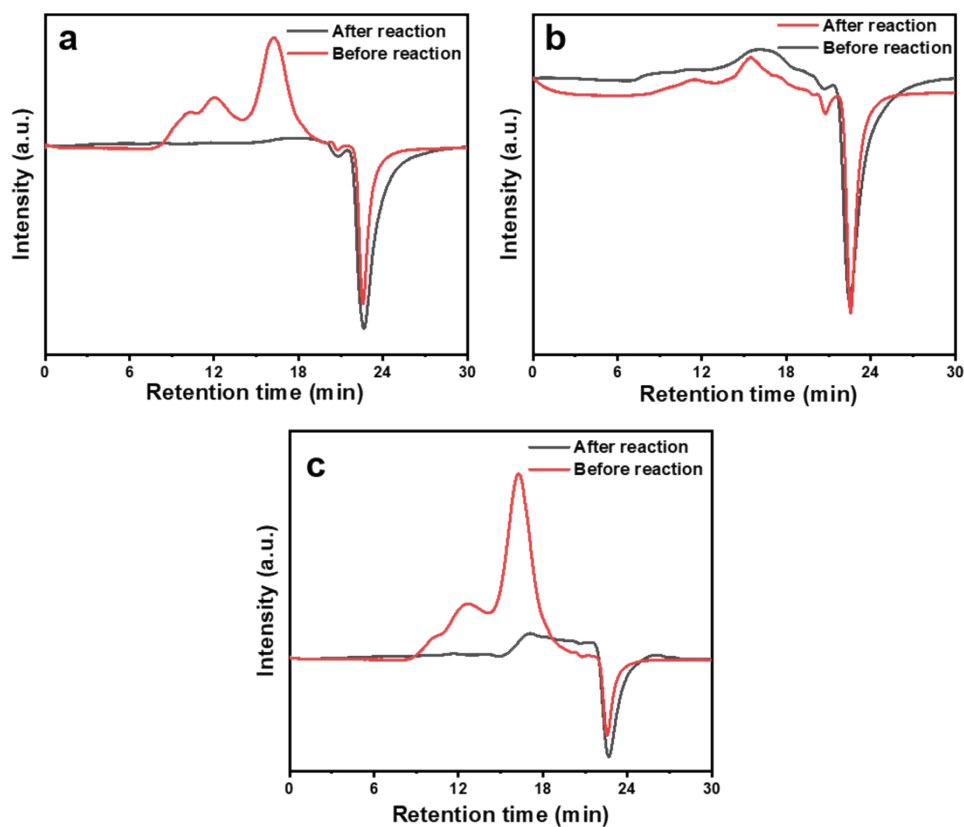|		M_w (Da)	M_n (Da)	PDI (M_w/M_n)
4				

Figure S8. GPC analysis of birch lignin (a), pine lignin (b) and wheat straw lignin (c) before and after photocatalytic reaction. Samples for GPC analysis were dissolved by DMF for 24 h at room temperature.

GPC was used for analysis of birch lignin, pine lignin and wheat straw lignin before and after illumination (Figure S8 and Table S4). Before reaction, the peak area at about 16 min are attributing to a higher molecular weight of lignin samples. After reaction, the larger molecular weight M_w decreased significantly and the peak area of low molecular weight increased, meaning that this photocatalytic system could effectively depolymerize lignin samples.
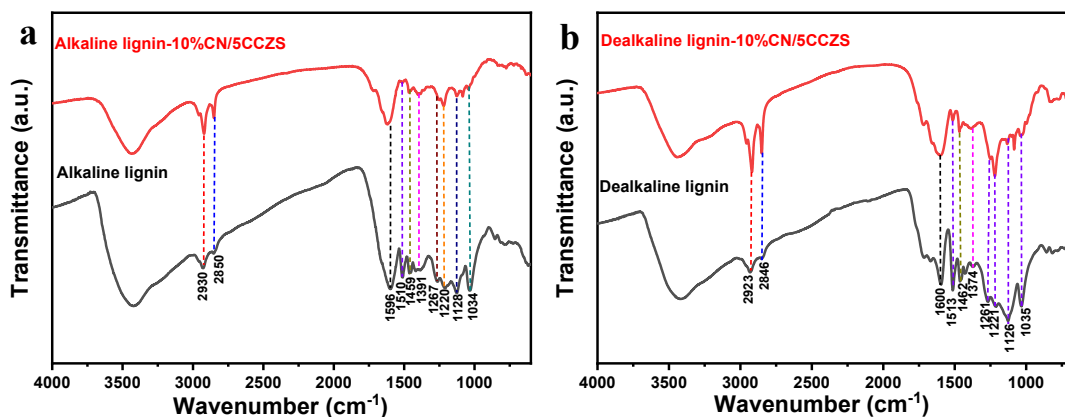
Figure S9. FT-IR spectra of alkaline (a) and dealkaline (b) after photocatalytic reaction.

Table S5. Assigned FT-IR peaks of alkaline and dealkaline lignin samples.

Wavenumber (cm^{-1})	Band assignment
2930/2923	C-H stretching vibration of -CH$_3$ in lignin
2850/2846	C-H stretching vibration of -CH$_2$- in lignin
1596/1600	C=C skeleton stretching of benzene skeleton
1510/1513	C=C stretching vibration of benzene skeleton
1459/1462	In-plane bending vibration of C-H bond
1391/1374	O-H bond in-plane bending vibrations of tertiary alcohols
1267/1261	O-H in-plane bending vibration of alcohols or phenols
1220/1221	C-O-C stretching vibration of esters
1128/1126	C-O bond stretching vibration of tertiary alcohol
1034/1035	R-C-O-stretching vibration of aryl ether

FT-IR analysis is used to investigated the types of functional groups in raw lignin (alkaline lignin and dealkaline lignin) and depolymerized products. The wide absorption band between 3200-3600 cm-1 is assigned to the O-H stretching of alcohols, phenols and absorbed water in raw lignin and depolymerization products. The bands at 2930/2923 and 2850/2846 cm-1 are assigned to C-H stretching vibration of -CH$_3$ and -CH$_2$-. The absorption peaks at 1596/1600 and 1510/1513 cm^{-1} are ascribed to C=C stretching of aromatic skeleton. The peak at 1459/1462 cm^{-1} is corresponded to in-plane bending vibration of C-H bond. The peaks at 1391/1374 and 1267/1261 cm^{-1} are ascribed to O-H bond in plane bending vibrations in lignin linkages or aromatic rings. The peaks during 1220/1221, 1128/1128 and 1034/1035 cm^{-1} are mainly due to C-O stretching in lignin linkages. Significant spectral changes of depolymerized products can be observed in the fingerprint region, suggesting that lignin was indeed depolymerized. Especially, this absorption peaks of all C-O bond almost disappeared after photocatalytic depolymerization compared with the remaining

characteristic absorption peaks of C=C bond at 1596/1600 cm-1 in the aromatic ring, indicating that the linkages between the aromatic rings have been cleaved and aromatic ring is retained.

Table S6. Photocatalytic depolymerization of lignin or sodium lignosulfonate in previous studies.

Cat.	Light source	Time (h)	Yield of vanillin (mg/g lignin or sodium lignosulfonate)	Photocatalytic efficiency (mg g^{-1} h^{-1})[a]	Ref.
TiO$_2$	λ > 350 nm	6	2.1	0.35	[10]
C$_{60}$/Bi$_2$TiO$_4$F$_2$	λ > 400 nm	12	5	0.42	[11]
M-TiO2/BiOI	λ > 400 nm	56	5.8	0.10	[12]
Bi-Pt/TiO$_2$	UV-vis	1	5	5.00	[13]
TiO$_2$/Lignin	365 nm	5	16.8	3.36	[14]
VO(OiPr)$_3$	455 nm	24	3.5	0.15	[15]
CdS/HPA-2/g-C$_3$N$_4$	Vis	4	23.8	5.95	[16]
Gd^{3+}: CeVO$_4$/P-Pal	NIR	6	4.5	0.75	[17]
CdS/BiOI-V$_I$	λ > 400 nm	6	10.95	1.83	[18]
MSCN-0.5	425 nm	6	7.30	1.22	[19]
CN/CQDs/CZS	Vis	2	26.1	13.05	This work

[a] Photocatalytic efficiency was calculated by a self-defined formula, Photocatalytic efficiency (mg g$_{lignin}$$^{-1}$ h^{-1}) =
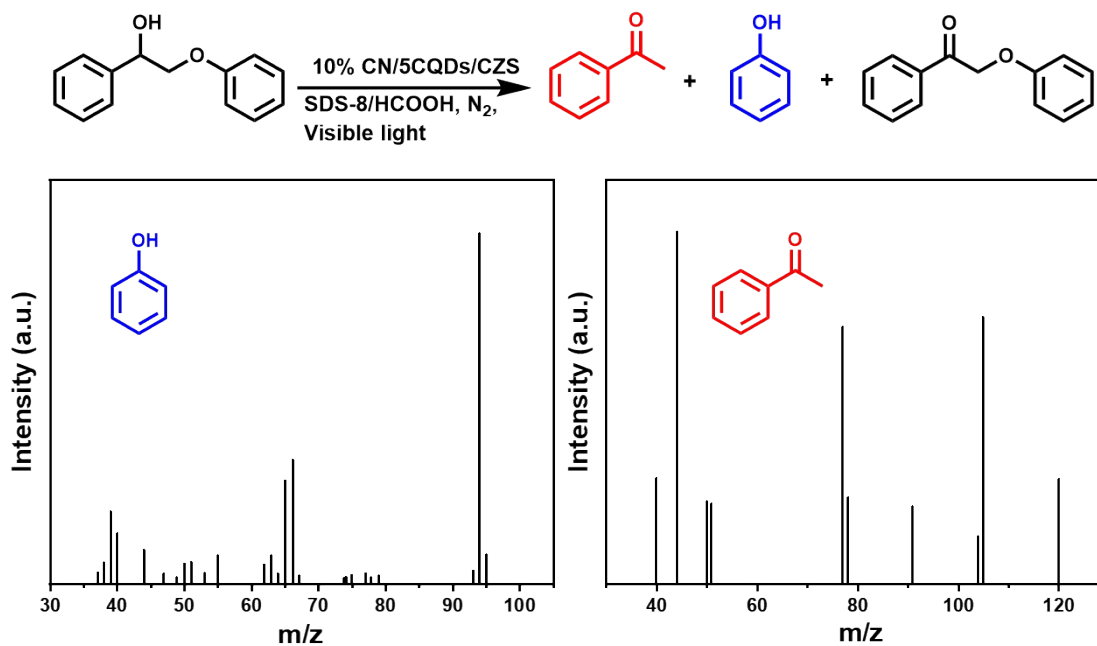
Yield of vanillin / reaction time.

Figure S10. Mass spectrograms of phenol and acetophenone measured by GC-MS. Reaction conditions: 5 mg PP-ol, 5 mg 10% CN/5CQDS/CZS, 5 mL of SDS-8/HCOOH (4/1, v/v), N_2 atmosphere, 300W Xe-lamp, 1.5 h.
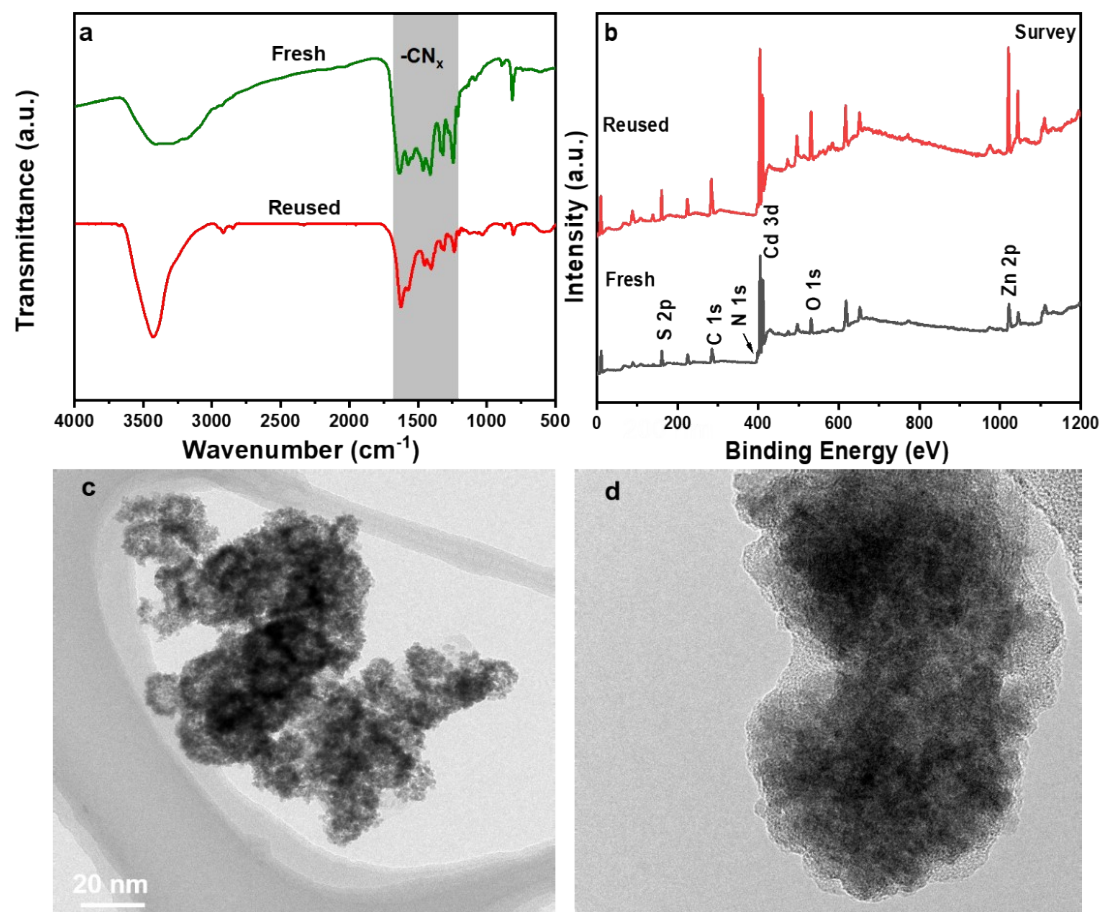
Figure S11. (a) FT-IR spectra and (b) XPS survey spectra of 10% CN/5CQDs/CZS before and after stability test, (c-d) TEM images of reused 10% CN/5CQDs/CZS.
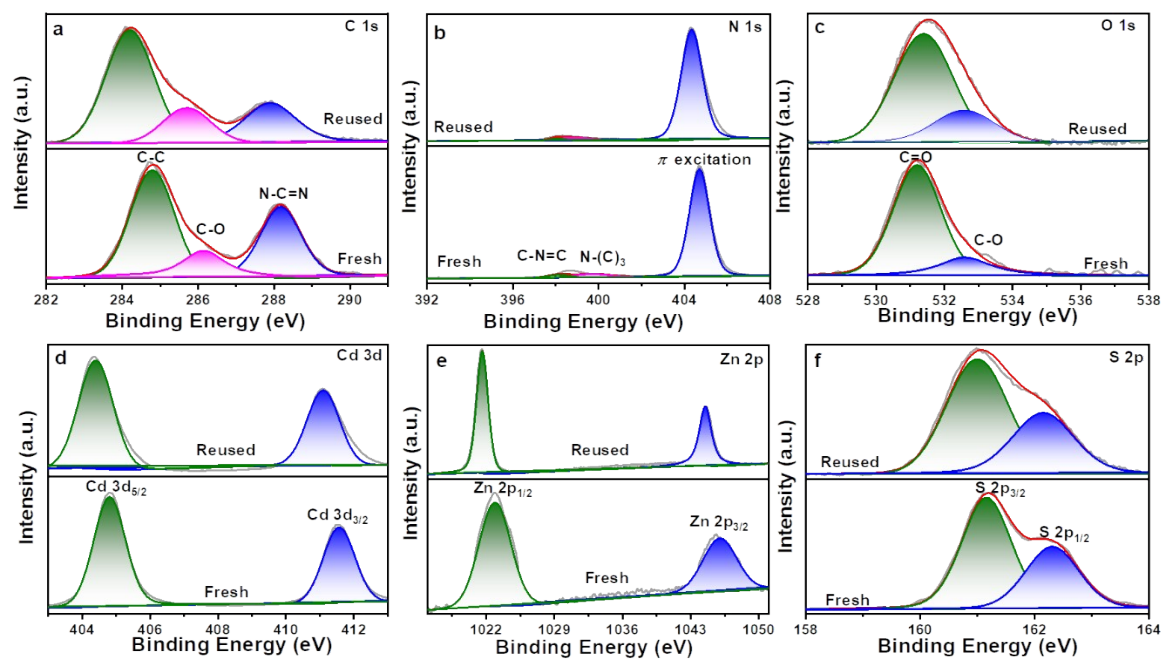
Figure S12. High-resolution XPS spectra of (a) C 1s, (b) N 1s, (c) O 1s, (d) Cd 3d, (e) Zn 2p, (f) S 2p for fresh and reused 10% CN/5CQDs/CZS.
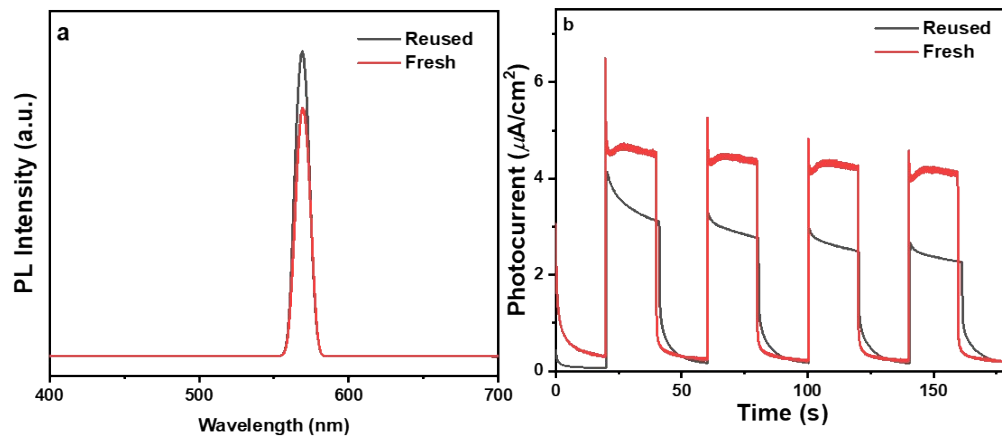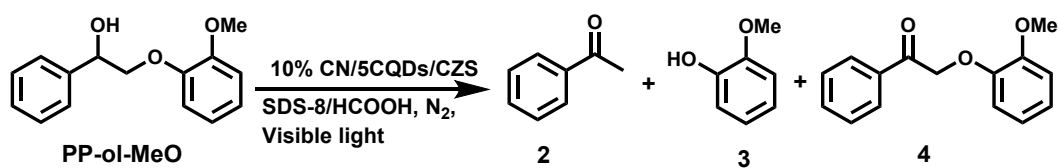
Figure S13. (a) PL and (b) transient photocurrent response of fresh and reused 10% CN/5CQDs/CZS.

Table S7. Photocatalytic conversion of the methoxyl-substituent lignin model compound.

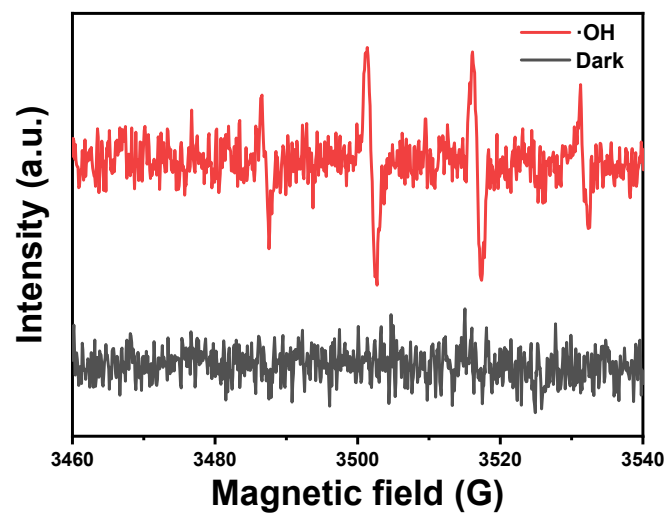| Catalyst	Substrate	Atmos.	Conv. (%)	Yield of products (%)			Selectivity of C-O bond cleavage (%)
				2	3	4	
10% CN/5CQDs/CZS	PP-ol-MeO	N_2	80	49.5	39.8	0	~100

Figure S14. DMPO-•OH spin-trapping ESR spectra in 10% CN/5CCZSCQDS/CZS.

Reference

1. G. Kresse and J. Furthmüller, *Phys. Rev. B*, 1996, **54**, 11169-11186.

2. J. P. Perdew, K. Burke and M. Ernzerhof, *Phys. Rev. Lett.*, 1996, **77**, 3865-3868.

3. G. Kresse and D. Joubert, *Phys. Rev. B*, 1999, **59**, 1758-1775.

4. A. Jain, O. Shyue Ping, G. Hautier, W. Chen, W. D. Richards, S. Dacek, S. Cholia, D. Gunter, D. Skinner, G. Ceder and K. A. Persson, *APL MATERIALS*, 2013, **1**, 011002.

5. H. J. Monkhorst and J. D. Pack, *Phys. Rev. B*, 1976, **13**, 5188-5192.

6. Y. Shao, Q. Xia, L. Dong, X. Liu, X. Han, S. F. Parker, Y. Cheng, L. L. Daemen, A. J. Ramirez-Cuesta, S. Yang and Y. Wang, *Nat. Commun.,* 2017, **8**, 16104.

7. D. Wang, M. Cui, Y. Li, W. Zhao, S. Ma, Z. Jiang, X. Liu, C. Liang, R. Li, L. Ma, Y. Song and X.-Y. Wei, *J. Agric. Food Chem.*, 2023, **71**, 2026-2037.

8. X. Liu, Z. Jiang, X. Cao, Z. Shen, W. Zhao, F. Wang, M. Cui and C. Liang, *ACS Sustain. Chem. Eng.*, 2023, **11**, 14947–14959.

9. M. Cui, D. Wang, Y. Li, W. Zhao, C. Liang, X. Liu, S. Fu, L. Wang and X. Wei, *New J. Chem.*, 2022, **46**, 4167-4178.

10. R. Prado, X. Erdocia and J. Labidi, *Chemosphere*, 2013, **91**, 1355-1361.

11. Z. Du, W. Li, Z. Xu, H. Wu, H. Jameel, H.-M. Chang and L.-L. Ma, *J. Wood Chem. Technol.*, 2016, **36**, 365-376.

12. J. Qiu, D. Dai, L. Zhang, Y. Zhou, L. Yang and J. Yao, *J. Colloid Interface Sci.,* 2022, **605**, 648-656.

13. J. Qiu, D. Dai, L. Zhang, M. Li, J. Xu and J. Yao, *Microporous Mesoporous Mat.*, 2021, **319**, 111043.

14. N. Srisasiwimon, S. Chuangchote, N. Laosiripojana and T. Sagawa, *ACS Sustain. Chem. Eng.*, 2018, **6**, 13968-13976.

15. H. F. Liu, H. J. Li, N. C. Luo and F. Wang, *ACS Catal.*, 2020, **10**, 632-643.

16. M. Cui, C. Liang, W. Zhao, X. Liu, L. Dong, D. Wang, S. Fu, Z. Jiang, F. Wang and X. Wei, *Fuel Process. Technol.,* 2022, **238**, 107481.

17. L. Sun, X. Ye, Z. Cao, C. Zhang, C. Yao, C. Ni and X. Li, *Appl. Catal. A-Gen.*, 2022, **648**, 118923.

18. D. Dai, J. Qiu, G. Xia, L. Zhang, H. Ma, L. Yang and J. Yao, *Int. J. Biol. Macromol.*, 2023,

227, 1317-1324.

19. C. Ku, H. Guo, K. Li, Q. Wu and L. Yan, *Chin. Chem. Lett.*, 2023, **34**, 107298.